Finite Wavelength Instabilities in a Slow Mode Coupled Complex Ginzburg-Landau Equation

M. Ipsen
UNI•C, Danish Computing Center for Research and Education, The Technical University of Denmark, Building 304, DK-2800 Lyngby, Denmark

P. G. Sørensen
Department of Chemistry, University of Copenhagen, H.C.Ørsted Institute, Universitetsparken 5, DK-2100 Copenhagen, Denmark

(February 5, 2008)

In this letter, we discuss the effect of slow real modes in reaction-diffusion systems close to a supercritical Hopf bifurcation. The spatio-temporal effects of the slow mode cannot be captured by traditional descriptions in terms of a single complex Ginzburg-Landau equation (CGLE). We show that the slow mode coupling to the CGLE, introduces a novel set of finite-wavelength instabilities not present in the CGLE. For spiral waves, these instabilities highly effect the location of regions for convective and absolute instability. These new instability boundaries are consistent with transitions to spatio-temporal chaos found by simulation of the corresponding coupled amplitude equations.

47.20.Ky, 52.35.Mw

Amplitude equations have been used in a variety of scientific contexts to describe spatio-temporal modulations of reference states close to the onset of criticality. In dynamical systems close to a supercritical Hopf bifurcation [1], the spatio-temporal modulation of the homogeneous stationary state can be described by the complex Ginzburg-Landau equation (CGLE). This applies to chemical and biochemical reaction-diffusion systems, among which the Belousov-Zhabotinsky (BZ) reaction is the most well known [2].

For chemical systems [3,4], one of the most striking features of the CGLE is its ability to exhibit spiral wave solutions (point defects) similar to experimental observations in a large number of chemical reaction-diffusion systems. Recently, it was shown [5] that the CGLE fails to model even qualitatively the dynamics of a realistic 4-species Oregonator model [6] of the BZ reaction. This discrepancy is caused by the presence of a slow real mode in the homogeneous part of the Oregonator model. By considering a slow-field coupling to the CGLE, we show how the inclusion of an amplitude equation for the slow mode gives rise to a finite-wavelength instability for plane waves which is not present in the CGLE. For spiral waves, we have calculated new boundaries for convective and absolute instability.

Here we consider reaction-diffusion systems whose spatio-temporal dynamics is governed by

$$\partial \mathbf{c}/\partial t = \mathbf{F}(\mathbf{c};\mu) + \mathbf{D}\cdot\nabla^2\mathbf{c}, \tag{1}$$

where $\mathbf{c} = \mathbf{c}(\mathbf{x},t)$ depends on the spatial position vector $\mathbf{x}$ and time t, and $\mathbf{D}$ is a diffusion matrix. Close to the onset of a supercritical Hopf bifurcation of a homogeneous solution of Eq. (1), the spatio-temporal modulation of this state can be described by the complex Ginzburg-Landau equation (CGLE). In dimensionless form, the CGLE can be written compactly as

$$\dot{w} = w - (1+\mathrm{i}\,\alpha)w|w|^2 + (1+\mathrm{i}\,\beta)\nabla^2 w. \tag{2}$$

As shown in [3], the two real coefficients, α and β, and the transformation from w to chemical concentration $\mathbf{c}$ can be derived rigorously from the original reaction-diffusion system (1). The CGLE admits plane wave solutions of the form $w(t,\mathbf{x}) = A\exp[\mathrm{i}(\mathbf{Q}\mathbf{x} - \omega t)]$, with amplitude $A = \sqrt{1-Q^2}$ and frequency ω determined by the dispersion relation $\omega = \beta Q^2 + (1-Q^2)\alpha$ (where $Q = |\mathbf{Q}|$). The stability of a given plane wave is determined by the growth rate $\lambda(k)$ of perturbations with $\mathbf{k} \parallel \mathbf{Q}$

$$\lambda(k) = -(k^2 + 2\,\mathrm{i}\,\beta k Q + A^2) \pm \sqrt{(1+\alpha)^2 - k^2 + 2\,\mathrm{i}\,\beta k Q + A^2)^2}. \tag{3}$$

In particular, at the Eckhaus border defined by

$$D_\parallel = 1 + \alpha\beta - 2(1+\alpha^2)Q^2/(1-Q^2) = 0, \tag{4}$$

a plane wave with given Q, will be unstable to long-wavelength perturbations if $D_\parallel(Q) < 0$; finally, all plane waves are rendered unstable at the Benjamin-Feir-Newell (BFN) instability [7] where $1 + \alpha\beta < 0$.

For simple oscillatory chemical systems, the CGLE shows an almost quantitative agreement with the spatio-temporal dynamics of the actual chemical system [8]. However, for more complicated models of the BZ reaction, we have previously described [5] how the CGLE fails even qualitatively to model characteristic time and length scales of the models. This disagreement is caused by the presence of a slow (near-critical) real mode. To incorporate the dynamics of the slow real mode into a description valid close to criticality, one may derive an amplitude equation similar to the normal form associated with a fold-Hopf bifurcation for homogeneous systems [9]. In dimensionless representation, the amplitude equations becomes

$$\dot{w} = w + (1 + \mathrm{i}\,\gamma)wz - (1 + \mathrm{i}\,\alpha_\mathrm{s})w|w|^2 + (1 + \mathrm{i}\,\beta)\nabla^2 w, \tag{5a}$$

$$\epsilon\dot{z} = \lambda_0 z + \kappa|w|^2 + \epsilon\delta\nabla^2 z, \tag{5b}$$

where w and z describe the complex and real amplitudes of the oscillatory and slow real mode respectively. The parameter λ_0 is the reciprocal timescale of the slow real mode and ϵ describes the distance to the Hopf bifurcation point. The resonant nonlinear coefficients α_s, γ, and κ can be derived by application of classical normal form theory [9]. We shall refer to the system (5) as the distributed slow-Hopf equation (DSHE). The DSHE may be considered as a "normal form" or prototype model for oscillatory reaction-diffusion systems with a slow real mode. It describes, for example, a realistic 4-species model for the BZ-reaction very well [5]. In the following, we shall use $\lambda_0 = -3.07\times10^{-4}$, $\gamma = -1.56$, $\kappa = -3.10\times10^{-4}$, and $\delta = 0.67$ as calculated for this model, whereas α_s, β, and ϵ are regarded as free parameters. The value of ϵ in a realistic experiment is of the order 10^{-3}.

Observe that the DSHE (5) cannot be rescaled to be fully independent of the distance ϵ from the Hopf bifurcation point: Except for a rescaling of the amplitude of w, the DSHE converges to the CGLE when $\epsilon \to 0$ or $\lambda_0 \to -\infty$. In either of these limits, the coefficient α_s is related to the nonlinear coefficient α in the CGLE by

$$\alpha_\mathrm{s} = (\alpha + \gamma\kappa/\lambda_0)/(1 + \kappa/\lambda_0). \tag{6}$$

In the adiabatic approximation where either the operating point is sufficiently close to the Hopf point (ϵ small) or when the real mode λ_0 becomes large and negative, we expect the dynamics of the DSHE to be fully described within the framework of the CGLE. However, the distance from the bifurcation point where the adiabatic approximation holds may very well be extremely small and very likely experimentally unrealizable.

The DSHE admits a family of plane wave solutions of the form

$$w(t,\mathbf{x}) = A\exp[\mathrm{i}(\mathbf{Q}\mathbf{x} - \omega t)], \qquad z(t,\mathbf{x}) = Z, \tag{7}$$

where $A = \sqrt{(1-Q^2)/(1+\kappa/\lambda_0)}$, $Z = -A^2\kappa/\lambda_0$, and the frequency ω given by the dispersion relation $\omega = \beta Q^2 + \alpha A^2$ with α given by Eq. (6).

To investigate the stability of the plane waves (7), we consider the growth rate $\sigma(k)$ of longitudinal perturbations with $\mathbf{k} \parallel \mathbf{Q}$. For the DSHE, an analytic evaluation of the spectrum of eigenvalues requires the solution of a cubic polynomial with complex coefficients, and is therefore not suitable for analytic evaluation. Instead, we may apply second order linear perturbation theory [10] to obtain a series expansion for the growth rates: For the first order correction to the Eckhaus criterion (4), we obtain for the DSHE

$$E_\parallel = D_\parallel + \frac{4(\alpha-\beta)(\alpha-\gamma)\kappa Q^2}{\lambda_0(\lambda_0+\kappa)}\epsilon = 0, \tag{8}$$

where $D_\parallel$ is the Eckhaus criterion (3) for the CGLE. For $Q = 0$, we observe that the BFN criterion also holds for the DSHE. For the CGLE, all plane waves are long-wavelength unstable when $1 + \alpha\beta < 0$. For the DSHE, this no longer holds, since a band of plane waves of finite wavenumber still remain stable at the BFN point when $\epsilon > -\lambda_0(\lambda_0+\kappa)/(2\kappa(1+\beta\gamma))$. This band of plane waves, however, can become unstable to finite-wavelength perturbations determined by the condition

$$F_\parallel = \mathrm{Re}\,\sigma'(k) = 0, \qquad |k| > 0. \tag{9}$$

For example, for a homogeneous plane wave ($Q = 0$), expansion of $\sigma(k)$ to lowest nontrivial order in ϵ and fourth order in k yields

$$\sigma(k) = -(1+\alpha\beta)k^2 \pm \tfrac{1}{2}\big[(1+\alpha^2)\beta^2 + 2\frac{\beta(1+\alpha\beta-\delta)(\alpha-\gamma)\kappa}{\lambda_0(\lambda_0+\kappa)}\epsilon\big]k^4. \tag{10}$$

For the CGLE, the long-wavelength instability will always be the first plane wave instability to occur for the plane wave with $Q = 0$. However for the DSHE this result no longer holds, since the coefficient of order k^4 in Eq. (10) changes sign when

$$\epsilon = \frac{(1+\alpha^2)\beta\lambda_0(\lambda_0+\kappa)}{2(1+\alpha\beta-\delta)(\alpha-\gamma)\kappa} \tag{11}$$

causing a finite-wavelength instability to take place. A similar result can be derived for general Q. A typical band of unstable wave numbers are shown in Fig. 1. We also observe that Eqs. (8) and (10) converges to the corresponding stability results of the CGLE in either of the adiabatic limits $\epsilon \to 0$ or $\lambda_0 \to -\infty$. The described scenario is illustrated in Fig. 2. In (a), $\epsilon = 10^{-4}$, we obtain qualitatively the same behavior as in the CGLE, where the band of Eckhaus stable plane waves vanish at the BFN point. In (b), $\epsilon = 2.0 \times 10^{-4}$, a finite-wavelength band now persists above the BFN point. In addition, a finite-wavelength instability emerges at two points from the Eckhaus curve (open circles on figure). As α increases, the corresponding instability curve exhibits a limit point (black circle); above this point, all plane waves are unstable. The variation along the finite instability curve of the marginally unstable wavenumber of the finite perturbation is shown in (c).

Similar to the CGLE, the DSHE admits spiral wave solutions (phase defects) in both one and two spatial dimensions. In two spatial dimensions, these may be expressed in polar coordinates (r, θ) as $w(r,\theta) = A(r)\exp(\mathrm{i}(\psi(r) - \theta - \omega t))$ and $z(r) = Z(r)$, where $A(r)$ and $\psi(r)$ are the amplitude and phase of the spiral wave respectively in the complex w component whereas $Z(r)$ is the amplitude of the slow z component. These three quantities must satisfy the boundary value problem

$$A(0) = \psi(0) = Z(0) = 0, \tag{12a}$$

$$\lim_{r\to\infty} A(r) = \sqrt{(1-Q_\mathrm{s}^2)/(1+\kappa/\lambda_0)}, \tag{12b}$$

$$\lim_{r\to\infty} Z(r) = -A(r)^2\kappa/\lambda_0 \tag{12c}$$

where $Q_\mathrm{s} = \lim_{r\to\infty}\psi'(r)$ is the unique wave number selected by the spiral wave. We now discuss the stability properties of spiral wave solutions of Eq. (12). In order to compare the results with the properties of the CGLE, we shall use the parameter α determined implicitly by Eq. (6) as the free parameter, whereas all other parameters in the DSHE (5) are kept fixed.

For large r, spiral waves resemble plane wave solutions of the form Eq. (7), and we may therefore expect that the spiral wave stability is governed by the corresponding stability for a plane wave with $Q = Q_\mathrm{s}$. The transitions where spiral waves become either Eckhaus unstable or unstable to finite-wavelength perturbations are therefore $D_\parallel(Q_\mathrm{s}) = 0$ or $F_\parallel(Q_\mathrm{s}) = 0$ respectively. However, as described in [11], spiral waves emit plane waves with a nonzero group velocity $\mathrm{Im}\,\partial\sigma/\partial k$, causing perturbations to drift away; the conditions (8) and (9) are conditions for convective instability, and can therefore only be taken as necessary criteria for instability. To determine exponential growth of a perturbation $u(\mathbf{x}, t)$ even in a steady coordinate frame, we must evaluate the Fourier integral

$$u(\mathbf{x},t) = \frac{1}{2\pi}\int_{-\infty}^{\infty} u_k(0)\mathrm{e}^{\mathrm{i}\,kx+\sigma(k)t}dk \tag{13}$$

for large t in the saddle-point approximation [12]. The crossing to absolute instability is then determined by the two conditions $\sigma'(k_0) = 0$ and $\mathrm{Re}\,\sigma(k_0) = 0$.

For four selected values of ϵ, we have determined the variation in the (α, β)-plane of the DSHE instability thresholds for Eckhaus, finite-wavelength, and absolute instability as shown in Fig. 3. To solve the associated highly unstable boundary value problem, we have used a continuation tool with support for multiple shooting [13]. The corresponding Eckhaus and absolute instability borders for the CGLE are also shown as indicated by the gray-shaded area. Even for ϵ small (a), the Eckhaus threshold deviates significantly from the corresponding CGLE curve whereas the absolute instability curve almost coincides with the CGLE result. Note that the finite-wavelength instability does not exist for this value of ϵ. However, as ϵ is increased (b-d), the finite-wavelength curve completely determines the onset of convective instability, and the Eckhaus curve has been omitted from these panels. We observe that both of the DSHE instability limits gradually are shifted to the left of the CGLE boundary. Finally, for $\epsilon = 10^{-3}$ (d), the instability limits lie completely outside of the limits predicted by the CGLE.

As observed for the CGLE [11,14], the absolute instability (AI) line, is indicative for the onset of persistent turbulence in the CGLE. Numerical simulations of the DSHE indicated by dots in Fig. 3b and 3d confirms a similar observation: spiral waves are convectively unstable below the AI line and absolutely unstable above the AI line, where

a transition to sustained turbulence is observed. A representative scenario for the DSHE close to the AI line in Fig. 3d is shown in Fig. 4.

The results derived in the stability analysis presented for the DSHE (5), show that the presence of a slow mode in oscillatory chemical reaction-diffusion systems, can give rise to a finite-wavelength instability of plane waves and spiral waves, which does not occur in the CGLE. In a real chemical system, this instability occurs at a value of ϵ where the amplitude of the oscillations is just below the limit of detection. So even close to the Hopf bifurcation point, this instability completely determines the stability of plane waves (which for the CGLE is given solely by the Eckhaus criterion Eq. (4)). As shown in both Figs. 3 and 2, the finite-wavelength instability has profound effects on the location of boundaries for convective and absolute stability for spiral waves, and completely alters the classical bifurcation diagram known for the CGLE as ϵ is increased.

For simple model systems of oscillatory chemical reaction-diffusion systems, such as the Brusselator [15] and the Gray-Scott model [16], the CGLE provides an almost quantitative description of spatio-temporal structures even at quite large distances from the bifurcation point; however, models of realistic chemical and biochemical systems, such as the BZ-reaction, the horseradish peroxidase system [17], and glycolytic oscillations [18,19] all posses one or more slow modes, and it is therefore unlikely that the CGLE will be applicable for modeling experimental observations on such systems.

We thank Igor Schreiber for valueable assistance with the calculations of the stability boundaries shown in Fig. 3.

---

[1] J. E. Marsden and M. McCracken, *The Hopf Bifurcation and Its Applications* (Springer-Verlag, New York, 1976).
[2] R. J. Field and M. Burger, *Oscillation and Travelling Waves in Chemical Systems* (Wiley-Interscience, New York, 1985).
[3] Y. Kuramoto, *Chemical Oscillations, Waves, and Turbulence* (Springer-Verlag, Berlin, 1984).
[4] R. Kapral, Physica D **86**, 149 (1995).
[5] M. Ipsen, F. Hynne, and P. G. Sørensen, to appear in *Physica D* (unpublished).
[6] J. Wang, P. G. Sørensen, and F. Hynne, Z. Phys. Chem. **192**, 63 (1995).
[7] A. C. Newell, Lectures in Appl. Math **15**, 157 (1974).
[8] M. Ipsen, F. Hynne, and P. G. Sørensen, Int. J. Bifurcation and Chaos **7**, 1539 (1997).
[9] J. Guckenheimer and P. J. Holmes, *Nonlinear Oscillations, Dynamical Systems and Bifurcations of Vector Fields* (Springer-Verlag, New York, 1983).
[10] T. Kato, *Perturbation Theory for Linear Operators* (Springer-Verlag, Berlin, 1966).
[11] I. S. Aranson, L. Aranson, L. Kramer, and A. Weber, Phys. Rev. A. **46**, R2992 (1992).
[12] J. Mathews and R. L. Walker, *Mathematical Methods of Physics* (W. A. Benjamin, Inc., New York, 1970).
[13] M. Marek and I. Schreiber, *Chaotic Behavior of Deterministic Dissipative Systems* (Cambridge University Press, Cambridge, 1995).
[14] H. Chate and P. Manneville, Physica A **224**, 348 (1996).
[15] R. Lefever and I. Prigogine, J. Chem. Phys. **48**, 263 (1968).
[16] P. Gray and S. K. Scott, J. Phys. Chem. **89**, 22 (1985).
[17] B. D. Aguda and R. Larter, J. Am. Chem. Soc. **113**, 7913 (1991).
[18] K. Nielsen, P. G. Sørensen, F. Hynne, and H.-G. Busse, Biophysical Chemistry **72**, 49 (1998).
[19] O. Richter, A. Betz, and C. Giersch, BioSystems **7**, 137 (1975).

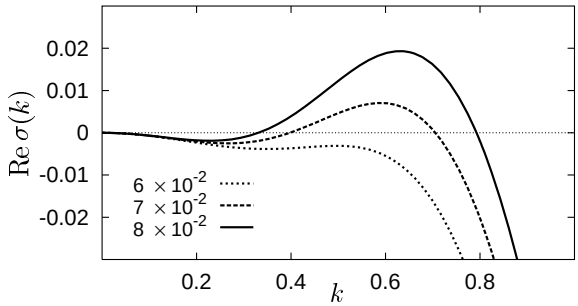

FIG. 1. Behavior of the real part of the most unstable eigenvalue $\sigma(k)$ for a plane wave solution of the DSHE for three different parameter values of the parameter ϵ close to criticality ($\alpha = 1.85$ and $\beta = -1$). The slow field coupling in Eq. (5) causes a finite-wavelength instability to occur before the onset of long-wavelength instabilities.

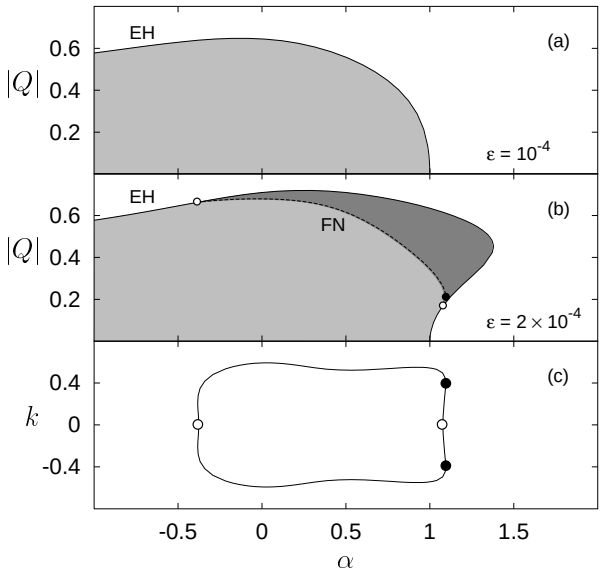

FIG. 2. (a) and (b) show curves in the $(|Q|, \alpha)$ plane describing Eckhaus (EH) and finite-wavelength (FN) instabilities of plan wave solutions of the DSHE (5) for two different values of ϵ and $\beta = -1$. (c) describes the variation along the FN curve in (b) of the marginally unstable wavenumber of the finite perturbation.

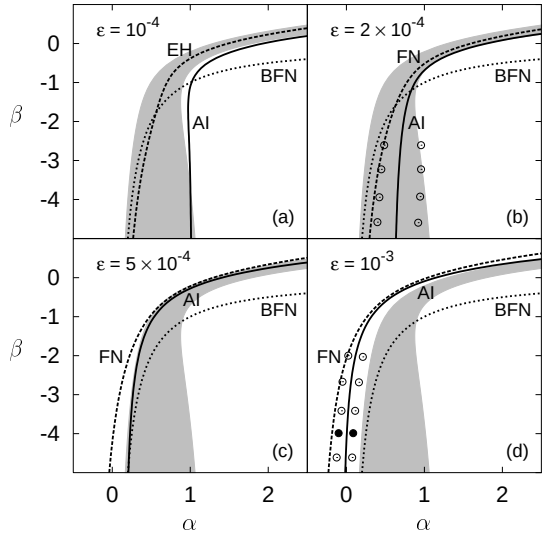

FIG. 3. Parameter diagrams showing the variation of the instability boundaries for spiral wave solutions of the DSHE (5) for four different values of the parameter ϵ. The figure shows the dominant boundaries for convective instabilities (dashed line), Eckhaus (EH) in (a) and finite-wavelength (FN) in (b-d), together with the boundary for absolute instabilities (AI, solid line). The left and right boundaries of the gray-shaded area indicate the Eckhaus and absolute instability curves for the CGLE respectively. The Benjamin-Feir-Newell line (BFN) is also shown. For (b) and (d), small circles indicate points where the behavior has been confirmed by direct simulation of the DSHE.

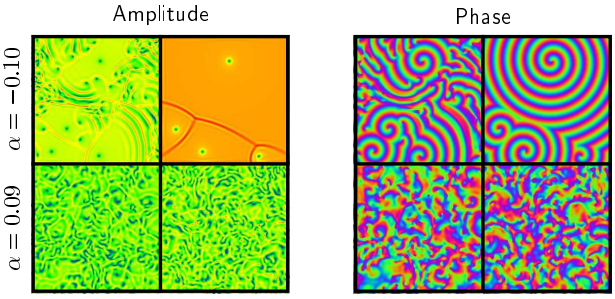

FIG. 4. Snapshots showing the behavior of the DSHE near the onset of absolute instability corresponding to the two parameter points indicated by filled circles in the bifurcation diagram in Fig. 3. For $\alpha = -0.10$, a convectively unstable transient ends in a frozen spiral state while $\alpha = 0.09$ gives rise to persistent spatio-temporal chaos.